Catalysis Science & Technology

ROYAL SOCIETY OF CHEMISTRY

PAPER

View Article Online
View Journal | View Issue

Cite this: *Catal. Sci. Technol.*, 2025, **15**, 1998

Formation of HCHO, CO and H_2 by methane oxidation with O_2 over Cu catalysts stabilized in silicoaluminophosphates†

Mana Shimakawa,[a] Rieko Nagase,[a] Ryoya Kugo,[a] Junya Ohyama [b] and Sakae Takenaka *[a]

Received 6th December 2024,
Accepted 28th January 2025

DOI: 10.1039/d4cy01469c

rsc.li/catalysis

The catalytic performance of Cu catalysts supported on SAPO34 (denoted as Cu/SAPO) for methane oxidation with O_2 has been investigated in detail. Cu/SAPO catalysts formed H_2 in addition to CO and HCHO during methane oxidation in the temperature range from 773 and 923 K, while the other 3d transition metal catalysts such as V, Cr, Mn, Fe, Co and Ni were less active for the formation of these products. The formation of HCHO, H_2 and CO was also confirmed during the reaction over Cu catalysts supported on zeolites different from SAPO34, such as mordenite, faujasite, chabazite, and beta-zeolite, but the yields of these products, especially the H_2 yield in the reaction over the Cu/SAPO catalyst, were significantly higher than those over other zeolite-supported Cu catalysts. In the oxidation over Cu/SAPO catalysts at 923 K, the yields of H_2, CO, and HCHO reached 2.2, 5.4, and 0.7%, respectively, at a methane conversion of 8.2%. These Cu catalysts were characterized by XRD patterns and *in situ* UV-vis spectra. Highly dispersed Cu^{2+} species stabilized in SAPO34 were the active sites for methane oxidation, which were reduced to Cu^{+} species by methane and oxidized to Cu^{2+} by O_2 to facilitate the reaction.

1. Introduction

Methane is distributed worldwide as a main component of natural gas and methane hydrate and it has been recognized as an abundant and clean energy resource.[1,2] Thus, methane has been utilized as an energy source for the supply of heat and the generation of electricity. On the other hand, the utilization of methane as a feedstock in the chemical industry has been limited. Methane has been converted into a synthesis gas composed of a mixture of CO and H_2 by reforming with H_2O or CO_2 (steam reforming or dry reforming) or partial oxidation with O_2.[3–5] Subsequently, synthesis gas can be converted to high value-added products such as methanol and hydrocarbons.[6–8] While steam reforming can produce synthesis gas with a composition that is effective for producing methanol, dry reforming can contribute to reducing greenhouse gas emissions. Huge energy input is required for the production of H_2 and CO through the reforming of methane with H_2O and CO_2 because their reactions are highly endothermic. Additionally, the reforming of methane has been operated at temperatures higher than 1073 K since methane is chemically inactive and has strong C–H bonds. The processes to produce methanol and hydrocarbons through the synthesis gas from methane thus need multiple steps inevitably. The direct conversion of methane by the oxidation with O_2 into methanol, formaldehyde, CO and H_2 is an ideal process from the viewpoint of green chemistry, because the reaction is exothermic and proceeds at low temperatures compared to steam reforming.[9,10] Many research groups have developed catalysts for the conversion of methane into oxygenates such as methanol and formaldehyde.[11–13] Methanol is formed by the oxidation of methane with O_2 over Cu catalysts stabilized in various zeolites at low temperatures (at around 550 K).[14–17] Atomically dispersed Cu oxides in zeolites such as mordenite and chabazite work as active sites for methanol formation. The reactions have been performed step by step, *i.e.*, Cu catalysts supported on zeolites are brought into contact with O_2 to form active oxygen species on the active sites, followed by being in contact with methane to form methoxy intermediates. Finally, the catalysts with intermediates are treated with water vapor to form methanol. Recently, it was demonstrated that methanol could be catalytically formed by contact of the Cu catalysts with mixed gases of methane, O_2 and water vapor, but the yield of methanol was very low.[18,19]

[a] *Department of Science and Engineering, Doshisha University, Tatara-miyakodani 1-3, Kyotanabe, Kyoto 610-0321, Japan. E-mail: stakenak@mail.doshisha.ac.jp*
[b] *Faculty of Advanced Science and Technology, Kumamoto University, 2-39-1 Kurokami, Chuo-ku, Kumamoto, 860-8555, Japan*

† Electronic supplementary information (ESI) available. See DOI: https://doi.org/10.1039/d4cy01469c

Recently, it was reported that a Ni catalyst supported on silicoaluminophosphate zeolite (SAPO-5) exhibited excellent catalytic performance for syngas production, and the performance was improved by the addition of Sr oxide.[20]

As for the partial oxidation of methane into formaldehyde, metal oxides such as V, Mo, Fe, and Cu supported on silica have been utilized as catalytically active components.[21] Atomically dispersed metal oxide clusters supported on silica work as active sites for formaldehyde formation by methane oxidation with O_2.[22] For example, a formaldehyde selectivity of 16% was reported at a methane conversion of 10% in the oxidation of methane over V_2O_5/SiO_2 at 903 K.[23] Some metal phosphates also show excellent catalytic performance for the formation of formaldehyde by methane oxidation with O_2.[24] Crystallized $FePO_4$ is the active catalyst for formaldehyde formation in methane oxidation at 673–823 K, showing a formaldehyde yield of around 0.3% at 823 K.[25,26] We have also reported that copper phosphate $Cu_2P_2O_7$ works as an active catalyst for the formation of formaldehyde through methane oxidation with O_2.[27] A formaldehyde yield of 1.0% could be obtained by methane oxidation over the $Cu_2P_2O_7$ catalyst at 923 K. Additionally, the catalytic performance of $Cu_2P_2O_7$ was improved by dilution with Al_2O_3 or deposition onto a SiO_2 support, due to the formation of smaller $Cu_2P_2O_7$ crystallites.[28] The $Cu_2P_2O_7$ catalysts modified with Al_2O_3 or SiO_2 showed higher formaldehyde yields and excellent durability for methane oxidation at 923 K, compared to the pure $Cu_2P_2O_7$ catalyst. We believe that highly dispersed Cu oxides surrounded with phosphate anions work as efficient active sites for methane oxidation with O_2 to form formaldehyde. In the present study, Cu oxides are supported on silicoaluminophosphate zeolite (SAPO34) (denoted as Cu/SAPO, hereafter), in order to form atomically dispersed Cu oxides which interact with phosphates. Because SAPO34 is composed of tetrahedral SiO_4, AlO_4, and PO_4 units, Cu cations should be surrounded with these units. We would report the formation of H_2 in addition to formaldehyde and CO with high yields by methane oxidation with O_2 over Cu/SAPO catalysts.

2. Experimental section

2.1 Preparation of catalysts

Supported Cu catalysts were prepared by a conventional impregnation method. Support materials were impregnated into an aqueous solution of $Cu(CH_3COO)_2$ at 363 K for 12 h and then dried up at 363 K. The samples were further dried at 363 K for 24 h in air. Finally, samples thus obtained were calcined at 973 K for 5 h in air. Mordenite (denoted as MOR, JRC-Z-HM20, SiO_2/Al_2O_3 = 18), beta-zeolite (denoted as *BEA, JRC-Z-B25, SiO_2/Al_2O_3 = 25), faujasite zeolite (FAU, JRC-Z-HY5.5, SiO_2/Al_2O_3 = 5.6), silica (SiO_2, JRC-SIO13), alumina (Al_2O_3, JRC-ALO8), chabazite (denoted as CHA, SiO_2/Al_2O_3 = 26) and SAPO34 (denoted as SAPO, $SiO_2/Al_2O_3/P_2O_5$ = 10/42/48) were used as supports. All the zeolite supports used in the present study were impregnated into an aqueous solution of NH_4-Cl, followed by calcination at 973 K, in order to obtain H^+-exchanged zeolites. V, Cr, Mn, Fe, Co, Ni, Pd or Rh catalysts supported on SAPO were also prepared with a similar method described earlier by using $(NH_4)VO_3$, $Cr(CH_3COO)_2$, $Mn(CH_3COO)_2{\cdot}4H_2O$, $Fe(CH_3COO)_2$, $Co(CH_3COO)_2{\cdot}4H_2O$, $Ni(NO_3)_2{\cdot}6H_2O$, $Pd(NO_3)_2$ or $RhCl_3{\cdot}3H_2O$, respectively. The loading of these metal cations in the supported catalysts was adjusted to 0.5 wt%, if otherwise noted.

2.2 Methane oxidation with O_2

Methane oxidation with O_2 was carried out with a conventional gas flow system with a fixed catalyst bed at atmospheric pressure. Catalyst powder (0.050 g) diluted with quartz sand (1.0 g) was loaded on the catalyst bed in a quartz reactor (inner diameter = 6 mm). Temperatures of the catalyst bed in the reactor were monitored using the thermocouples installed in the reactor, which were in contact with the catalyst powder directly. The catalysts were treated with O_2 ($P(O_2)$ = 20 kPa) diluted with Ar at 973 K for 1 h prior to methane oxidation. Mixed gases composed of CH_4, O_2 and Ar ($CH_4:O_2:Ar$ = 2 : 1 : 5 as a volume ratio, the total flow rate = 70 mL min^{-1}) were introduced into the reactor and brought into contact with the catalysts for methane oxidation. Outlet gases from the reactor were passed through two traps cooled at *ca.* 273 and 200 K to condense a part of the products (HCHO and H_2O). Gases through the traps (H_2, CO and CO_2) were analyzed by GC with Porapak Q and active carbon columns for the evaluation of their formation rates. The concentration of HCHO condensed in the two traps was evaluated using UV-vis spectroscopy (UV/vis: V-650 spectrometer, Jasco). The products in the cold traps were added to mixed aqueous solutions of ammonium acetate, acetic acid and acetylacetone at 353 K, to form 3,5-diacetyl-1,4-dihydrolutidine prior to the measurement of the UV-vis spectra.[29] The concentration of HCHO was evaluated from the absorption at 413 nm due to 3,5-diacetyl-1,4-dihydrolutidine formed from HCHO. The liquid products were also analyzed by NMR, but the formation of methanol was not confirmed in the oxidation of methane with O_2 over the catalysts tested in the present study.

Conversion of CH_4(O_2) was defined as follows,

$$\text{Conversion of } CH_4(\text{or } O_2)/\% = (\text{reaction rate of } CH_4(\text{or } O_2)) \times 100/(\text{flow rate of } CH_4(\text{or } O_2) \text{ introduced into the reactor})$$

Two types of selectivity, *i.e.* selectivity based on C or based on H in methane, were defined as follows (using selectivity to HCHO as an example)

$$\text{Selectivity to HCHO based on C}/\% = (\text{formation rate of HCHO}) \times 100/(\text{reaction rate of } CH_4)$$

Selectivity to HCHO based on H/% = (formation rate of HCHO × 2) × 100/(reaction rate of CH_4 × 4)

Selectivity to H_2O based on H was evaluated stoichiometrically from the formation rates of CO, CO_2, HCHO and H_2 and the reaction rates of CH_4 and O_2, since it was difficult to accurately evaluate the amount of H_2O using GC. The yield of each product can be calculated as the product of the conversion of CH_4 and the selectivity to the corresponding product.

2.3 Characterization of catalysts

Powder X-ray diffraction (XRD) patterns of the catalysts were measured at room temperature (Rigaku MiniFlex, Cu Kα radiation, λ = 1.5418 Å). The crystal phases of the catalysts were identified using the powder diffraction file (PDF) database of the International Centre for Diffraction Data (ICDD). *In situ* UV-vis diffuse reflectance spectra were measured using a UV-vis spectrometer (V-750, Jasco) with an *in situ* flow cell (VHR-764B, Jasco) having a quartz cell window.[30] Catalyst samples or $BaSO_4$ powder for the measurement of the background spectrum were loaded on a stainless pan (inner diameter of 7.1 mm, height of 4.1 mm). Cu catalysts were treated under an O_2 flow at 973 K for 30 min and then cooled to 773 K under N_2 prior to the measurement of UV-vis spectra. Diffuse reflectance UV-vis spectra of the catalyst samples were obtained after exposing the samples into mixed gases composed of CH_4, O_2 and N_2 at 773 K.

3. Results and discussion

3.1 Methane oxidation over various catalysts

Table 1 shows the results of the oxidation of methane with O_2 over different metal catalysts supported on SAPO. Aqueous solutions containing V, Cr, Mn, Fe, Co, Ni, Cu, Pd or Rh

Table 1 Methane oxidation over various metal catalysts supported on SAPO

		Conv./%		Sel. C-base/%			Sel. H-base/%			Yield/%		
Metal	Temp./K	CH_4	O_2	HCHO	CO	CO_2	HCHO	H_2	H_2O	HCHO	CO	H_2
Cu	773	0.9	2.2	21	54	24	11	28	62	0.2	0.5	0.3
	823	2.2	5.1	15	55	30	8	31	62	0.3	1.2	0.7
	873	4.9	10.2	11	60	29	6	29	66	0.6	2.9	1.4
	923	8.2	21.5	9	66	25	5	26	69	0.7	5.4	2.2
None (SAPO)	773	0.1	0.2	0	100	0	0	6	94	0.0	0.1	0.0
	823	0.2	0.4	0	67	33	0	10	90	0.0	0.1	0.0
	873	0.2	0.6	1	31	68	1	13	86	0.0	0.1	0.0
	923	0.5	1.9	1	11	88	1	6	93	0.0	0.1	0.2
V	773	0.2	0.5	0	100	0	0	2	97	0.0	0.2	0.0
	823	0.1	0.5	2	66	32	1	8	91	0.0	0.1	0.0
	873	0.2	0.7	5	29	66	2	11	87	0.0	0.1	0.0
	923	0.7	2.5	5	6	89	3	6	92	0.0	0.0	0.0
Cr	773	0.9	3.2	1	67	32	0	3	96	0.0	0.6	0.0
	823	2.1	7.5	1	57	42	0	3	96	0.0	1.2	0.1
	873	5.4	19.5	1	54	45	0	2	97	0.0	2.9	0.1
	923	11.6	44.4	0	56	43	0	2	98	0.0	6.5	0.2
Mn	773	0.4	1.4	2	71	27	1	3	96	0.0	0.3	0.0
	823	0.4	1.4	4	34	62	2	6	92	0.0	0.1	0.0
	873	0.6	2.4	4	17	80	2	9	90	0.0	0.1	0.1
	923	1.2	4.5	3	7	89	2	8	90	0.0	0.1	0.1
Fe	773	0.1	0.3	3	56	41	2	19	79	0.0	0.1	0.0
	823	0.2	0.5	4	29	67	2	27	70	0.0	0.0	0.0
	873	0.4	1.2	4	12	84	2	25	73	0.0	0.0	0.1
	923	0.9	3.1	4	5	91	2	20	78	0.0	0.0	0.2
Co	773	0.4	0.2	1	57	42	0	23	76	0.0	0.2	0.1
	823	0.5	1.8	1	11	88	0	15	85	0.0	0.1	0.1
	873	0.8	2.8	1	5	93	1	13	86	0.0	0.0	0.1
	923	1.2	4.5	2	6	92	1	15	84	0.0	0.1	0.2
Ni	773	0.1	0.3	3	41	56	2	18	81	0.0	0.0	0.0
	823	0.3	0.9	3	20	77	2	20	79	0.0	0.1	0.1
	873	0.7	2.5	3	7	90	1	15	83	0.0	0.1	0.1
	923	1.7	5.3	3	39	58	2	25	73	0.1	0.6	0.4
Pd	623	0.2	0.9	0	6	94	0	0	100	0.0	0.0	0.0
	673	1.1	4.4	0	2	98	0	0	100	0.0	0.0	0.0
	723	2.4	9.5	0	1	99	0	0	100	0.0	0.0	0.0
	773	23.5	99.0	0	17	83	0	12	88	0.0	4.0	2.7
Rh	673	2.1	8.3	0	4	96	0	0	100	0.0	0.1	0.0
	723	3.9	15.9	0	1	99	0	0	100	0.0	0.0	0.0
	773	21.1	91.9	0	7	93	0	3	97	0.0	1.4	0.7
	823	25.9	99.4	0	26	74	0	25	75	0.0	6.6	6.5

cations were impregnated into SAPO followed by calcination in air at 973 K. XRD patterns of these catalysts are shown in Fig. S1.† In the XRD patterns of all the catalysts, strong diffraction lines due to SAPO34 were observed at 2θ = 9, 13, 16, 21 and 31 degrees (PDF card No. 00-047-0630). Any diffraction lines assignable to compounds containing metals added into SAPO were not found in these XRD patterns. Metal species in these catalysts are thus suggested to be highly dispersed on SAPO.

The catalytic activity of SAPO for methane oxidation was significantly low as shown in Table 1. Metal cations added to SAPO should work as active sites for the reaction. Pd and Rh catalysts catalyzed methane oxidation to form CO_2 and H_2O in lower temperature ranges compared to the other catalysts shown in Table 1, indicating the higher activity of the former catalysts for the total oxidation of methane. CO and H_2 were also formed in the reaction over Pd and Rh catalysts at high temperatures. As described below in detail, CO and H_2 should be formed by reforming of methane with H_2O and/or CO_2 over these catalysts. In contrast, HCHO and CO in addition to CO_2 were formed in the temperature range from 773 to 923 K over the 3d transition metal catalysts tested in the present study. Cr and Cu on SAPO showed higher catalytic activity for the oxidation of methane with O_2, compared to the other 3d transition metal catalysts, as shown in Fig. 1(a). Although the catalytic activity of Cu/SAPO was similar to that of Cr/SAPO, the selectivity to HCHO over the former catalysts was significantly higher than that over the latter ones (Fig. S2†). As the reaction temperature increased in the reaction over the Cu/SAPO catalyst, the selectivity to HCHO decreased, and that to CO increased instead, suggesting that HCHO was converted into CO over the Cu/SAPO catalyst. It should be noted that the HCHO yield in the reaction over the Cu/SAPO catalyst was extremely higher than those over the other catalysts, as shown in Fig. 1(b). The HCHO yield for Cu/SAPO was as high as that in the reaction over crystallized $Cu_2P_2O_7$ catalysts, which were one of the most active catalysts for HCHO formation by methane oxidation with O_2.[27] Cu cations supported on SAPO should interact with PO_4 units in SAPO, similar to those in $Cu_2P_2O_7$.[27,28] Highly dispersed Cu cations chemically interacting with phosphates (PO_4) would be effective for the formation of HCHO in methane oxidation with O_2.

Surprisingly, the formation of H_2 was confirmed during the reaction over the Cu/SAPO catalyst, although a substantial amount of gaseous O_2 remained in the reactants due to low O_2 conversion (Table 1). The selectivity to H_2 was relatively high (28%) in the reaction over the Cu/SAPO catalyst at 773 K, and it did not decrease with the reaction temperature (Fig. S2d†). In contrast, in the case of the reaction over the Pd and Rh catalysts, H_2 and CO were only observed once nearly all gaseous O_2 was consumed (Table 1). The reaction behavior over the Pd and Rh catalysts aligns with that over previously reported conventional catalysts active for the production of synthesis gas such as supported Ni catalysts.[31–35] In these catalysts, H_2 and CO are produced *via* the indirect path: O_2 is completely consumed at the upper parts of the catalyst bed in the flow reactors to form CO_2 and H_2O and then the remaining methane is converted into CO and H_2 by reforming of methane with H_2O and/or CO_2 at the lower parts of the catalyst bed. Additionally, CO and H_2O are formed from CO_2 and H_2 (reverse water gas shift reaction). The reaction behavior over the Cu/SAPO catalyst differs significantly from that over the conventional catalysts. The formation of H_2 and CO at low O_2 conversions over the Cu/SAPO catalyst indicates that these products are formed through a different mechanism than the reforming of methane.

The catalytic performance of Cu/SAPO for methane oxidation with O_2 was compared with those of V, Cr, Mn, Fe, Co or Ni catalysts supported on SAPO in detail. The results are also shown in Table 1, Fig. 1 and S2.† The catalytic activity of Cr/SAPO was similar to that of Cu/SAPO, while the activity of the other catalysts was very low. All the 3d transition metal catalysts in Table 1 also formed HCHO, CO, CO_2 and H_2 during the reactions, but the selectivity to each product was strongly dependent on the type of metal which worked as the catalytically active site. Selectivities to HCHO, CO and H_2 in the reaction over the Cu/SAPO catalyst were relatively higher in the whole temperature range (773–923 K) compared to those over the other catalysts. The selectivity to HCHO was also higher in the reaction over V/SAPO and the selectivities to H_2 and CO were higher in the reactions over Co/SAPO and Ni/SAPO catalysts. However, these catalysts had much lower activity for methane oxidation, compared to the Cu/SAPO catalyst as shown in Fig. 1(a). When compared at the same methane conversion, the selectivities to HCHO and H_2 over the Cu/SAPO catalyst were higher than those over the

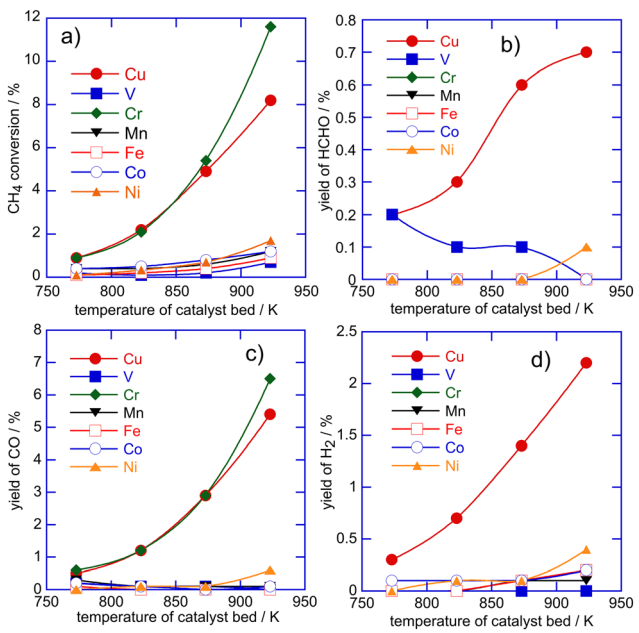

Fig. 1 Methane oxidation with O_2 over different metal catalysts supported on SAPO catalysts. a) CH_4 conversion, b) yield of HCHO, c) yield of CO and d) yield of H_2.

other metal catalysts (Fig. S3†). Thus, the yields of HCHO, CO and H_2 were appreciably higher in the reaction over the Cu/SAPO catalyst than those over the other catalysts (Fig. 1). The yield of HCHO, CO and H_2 was evaluated to be 0.7, 5.4 and 2.2%, respectively, at the methane conversion of 8.2% in the reaction over the Cu/SAPO catalyst at 923 K. It is meaningful that 74% of C atoms and 31% of H atoms in CH_4 molecules consumed by the oxidation with O_2 are utilized for the production of HCHO, CO and H_2 in the reaction over the Cu/SAPO catalyst. We concluded that Cu cations stabilized in SAPO showed excellent catalytic performance for the partial oxidation of methane with O_2 to form HCHO, CO and H_2. Recently, Murata and Hosokawa *et al.* investigated the catalytic performance of various metal oxides for the partial oxidation of methane with O_2.[36] The ZrO_2 catalyst showed the highest yield of synthesis gas in the reaction among 31 metal oxides tested in the study. ZrO_2 catalyzed the partial oxidation of methane into synthesis gas through the direct path. Kobayashi also reported the partial oxidation of methane with O_2 into H_2 and CO over Rh–Re catalysts supported on Al_2O_3 through the direct path.[37] They proposed that formates were formed on ZrO_2 or low-valent ReO_x species during methane oxidation with O_2 and the intermediates were decomposed into CO, CO_2 and H_2. Additionally, Kobayashi *et al.* demonstrated that CO was formed by the partial oxidation of methane with O_2 over the Re catalyst supported on mordenite to form CO through the direct path.[38] In these previous studies, the formation of HCHO was not confirmed during methane oxidation with O_2, while a high HCHO yield was obtained in the reaction over the Cu/SAPO catalyst. It is likely that different intermediates on the ZrO_2 or Re catalyst are formed on Cu cations stabilized on SAPO during methane oxidation.

In order to clarify the origin of superior catalytic performance of Cu/SAPO for the formation of HCHO, H_2 and CO in methane oxidation with O_2, the catalytic performance of Cu catalysts supported on different zeolites such as mordenite (denoted as MOR, hereafter), chabazite (CHA), beta-zeolite (*BEA) and faujasite zeolite (FAU) was evaluated. The results for the reactions are listed in Table 2. The Cu loading was adjusted to be 0.5 wt% for all the Cu catalysts in Table 2. XRD patterns for these Cu catalysts are shown in Fig. S4.† Only diffraction lines due to the corresponding zeolites were observed in the XRD patterns for these catalysts, suggesting the presence of highly dispersed Cu species for all the Cu catalysts in Table 2. All the Cu catalysts supported on these zeolites catalyzed methane oxidation with O_2 to form HCHO, CO, CO_2, H_2 and H_2O, similar to the Cu/SAPO catalyst, but the conversion of methane and the selectivity to each product strongly depended on the type of zeolite. No CH_3OH formation was observed at high temperatures such as 773 K during methane oxidation over any of the Cu catalysts in Table 2. The catalytic activity for the reaction was higher in the order of Cu/SAPO > Cu/MOR ≈ Cu/CHA >> Cu/*BEA > Cu/FAU as shown in Fig. 2. Cu/SAPO and Cu/MOR which had higher activity for methane oxidation tended to show

Table 2 Methane oxidation over Cu catalysts supported on different supports

		Conv./%		Sel. C-base/%			Sel. H-base/%			Yield/%		
Support	Temp./K	CH_4	O_2	CO	CO_2	HCHO	H_2	HCHO	H_2O	HCHO	CO	H_2
SAPO	773	0.9	2.2	54	24	21	28	11	62	0.2	0.5	0.3
	823	2.2	5.1	55	30	15	31	8	62	0.3	1.2	0.7
	873	4.9	10.2	60	29	11	29	6	66	0.6	2.9	1.4
	923	8.2	21.5	66	25	9	26	5	69	0.7	5.4	2.2
*BEA	773	0.2	0.5	57	9	35	17	17	66	0.1	0.1	0.0
	823	0.3	0.8	38	27	35	0	17	83	0.1	0.1	0.0
	873	0.7	2.1	30	41	30	5	15	80	0.2	0.2	0.0
	923	1.7	4.9	46	32	22	6	11	83	0.8	0.4	0.1
MOR	773	0.7	1.8	56	28	17	22	8	70	0.1	0.4	0.2
	823	1.8	4.1	52	33	15	19	7	73	0.3	0.9	0.4
	873	3.6	8.4	49	40	11	17	6	78	0.4	1.8	0.6
	923	5.7	16.0	62	29	9	16	5	79	0.5	3.5	0.9
FAU	773	0.1	0.3	70	0	30	0	15	85	0.0	0.0	0.0
	823	0.1	0.5	54	0	35	0	17	83	0.0	0.1	0.0
	873	0.3	1.2	49	11	35	7	17	76	0.0	0.1	0.1
	923	0.7	2.9	57	16	24	7	12	81	0.0	0.4	0.2
CHA	773	0.4	0.8	63	0	37	17	18	64	0.1	0.2	0.1
	823	1.2	2.2	57	15	28	23	14	63	0.3	0.7	0.3
	873	2.9	6.1	67	14	19	24	10	67	0.6	2.0	0.7
	923	5.4	12.4	73	11	16	24	8	68	0.9	3.9	1.3
Al_2O_3	773	0.8	1.4	63	37	0	24	0	76	0.0	0.5	0.2
	823	2.1	6.2	52	48	0	15	0	85	0.0	1.1	0.3
	873	5.2	15.6	46	54	0	10	0	90	0.0	2.4	0.5
	923	11.8	39.2	42	58	0	7	0	93	0.0	4.9	0.8
SiO_2	773	0.4	2.1	27	66	6	0	3	97	Tr	0.1	0.0
	823	0.7	3.2	17	48	36	2	18	80	0.3	0.1	Tr
	873	0.7	3.5	33	56	11	3	5	92	0.1	0.3	Tr
	923	1.2	5.2	38	41	21	3	11	86	0.3	0.5	Tr

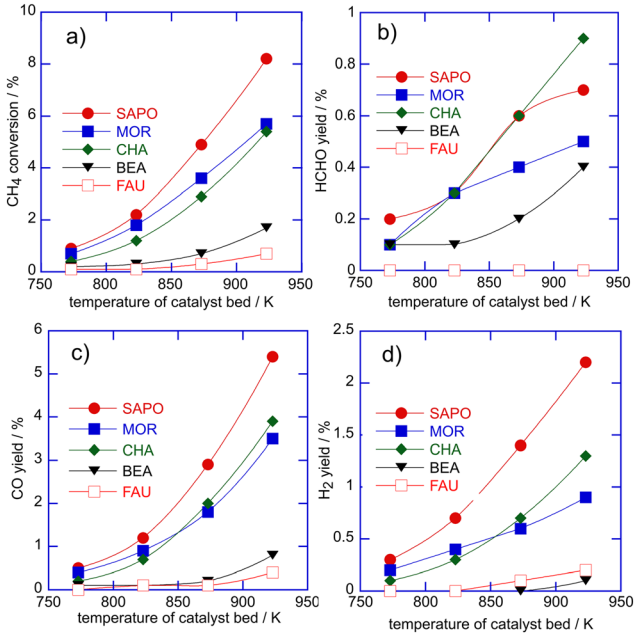

Fig. 2 Methane oxidation with O_2 over Cu catalysts supported on different zeolites. a) CH_4 conversion, b) yield of HCHO, c) yield of CO and d) yield of H_2.

lower selectivity to HCHO and higher selectivity to CO_2 as shown in Fig. S5.† In contrast, the selectivity to H_2 was the highest in the reaction over the Cu/SAPO catalyst although the catalyst had the highest activity among all the catalysts shown in Table 2. Thus, the yields of HCHO, CO and H_2 were relatively higher in the reaction over the Cu/SAPO catalyst compared to their yields over the other Cu catalysts. In particular, the H_2 yield for the Cu/SAPO catalyst was significantly higher than those for the other Cu catalysts. It is likely that interaction of atomically dispersed Cu cations with PO_4 units in zeolites results in the formation of active sites for H_2 production in the methane oxidation with O_2.

Methane oxidation with O_2 was also performed over Cu catalysts supported on SiO_2 and Al_2O_3. The loading of Cu for both catalysts was adjusted to 0.5 wt% similar to that for the Cu/SAPO catalyst. The results for the reactions over these Cu catalysts are also shown in Table 2. In the XRD patterns for both catalysts, very weak peaks due to CuO were observed at 2θ = 35 and 39 degrees in addition to broad peaks due to the supports as shown in Fig. S6.† Cu species in these catalysts are present as small crystallites of CuO in addition to highly dispersed Cu oxides.[39] The Cu/Al_2O_3 catalyst showed a similar activity for the reaction to the Cu/SAPO catalyst, whereas the catalytic activity of Cu/SiO_2 was very low. The selectivity to HCHO was high in the reaction over the Cu/SiO_2 catalyst, but that to H_2 was extremely low. Wang *et al.* reported that highly dispersed Cu oxides on mesoporous silica catalyzed the partial oxidation of methane with O_2 into HCHO.[40] Highly dispersed Cu oxides on silica should form HCHO through methane oxidation, while CuO crystallites catalyzed the total oxidation of methane into CO_2.[27] In methane oxidation over the Cu/Al_2O_3 catalyst, the formation of HCHO was not observed but selectivities to CO and H_2 were relatively high. From the results described earlier, we concluded that Cu cations stabilized on zeolites formed HCHO, CO and H_2 with high yields by methane oxidation with O_2.

Direct oxidation of methane with O_2 into methanol over Cu catalysts supported on zeolites such as CHA, MOR and ZSM-5 has been investigated by many research groups. Monomers or dimers of Cu stabilized in zeolites are believed to be active sites for methanol formation in the reaction.[30,41–43] Generally, highly dispersed Cu species stabilized in zeolites are activated with gaseous O_2 to form oxygen species active for methanol formation before the catalysts come into contact with methane in the temperature range from 473 to 573 K.[44] Formation of methanol is observed by the treatment of the catalysts with water vapor. High selectivity to methanol has been attained by the step-by-step reactions over these Cu catalysts, but the yield of methanol is extremely low due to low conversion of methane at low temperatures such as 473–573 K. In contrast, we performed methane oxidation with O_2 without water cofed in a higher temperature range from 773 to 923 K, to form H_2 in addition to HCHO, CO and CO_2. Highly dispersed Cu species in zeolites should also work as active sites for methane oxidation with O_2 to form HCHO, CO and H_2 in the present study, because any diffraction lines due to crystallized Cu compounds were not observed in the XRD patterns for these Cu catalysts. Note that the crystal structure of SAPO (SAPO34) is the same as that of CHA, although the atomic component of SAPO (Si, Al, P and O) is different from that of CHA (Si, Al and O). As described hereafter, UV-vis spectra for Cu/SAPO and Cu/CHA showed the presence of atomically dispersed

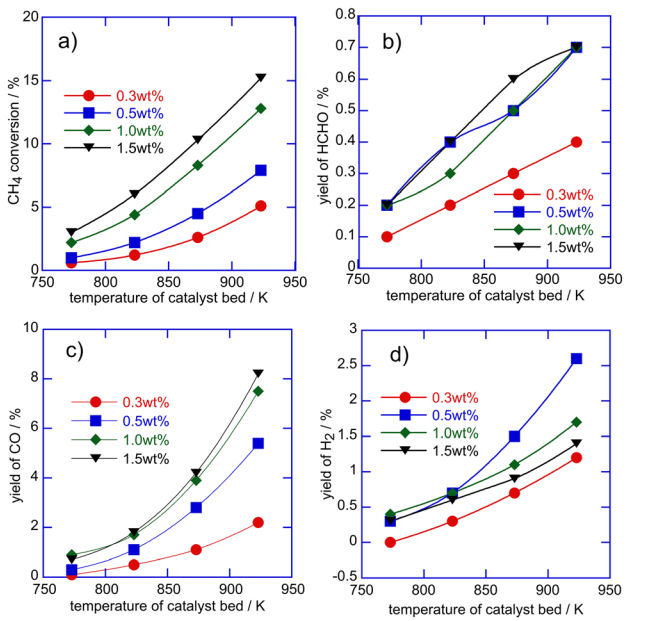

Fig. 3 Methane oxidation with O_2 over Cu/SAPO catalysts with different Cu loadings. a) CH_4 conversion, b) yield of HCHO, c) yield of CO and d) yield of H_2.

Cu^{2+}. The Cu cations in Cu/SAPO should be surrounded with lattice oxygen atoms in SiO_4, AlO_4 and PO_4 units, while Cu cations in the other zeolite-supported catalysts are in contact with SiO_4 and AlO_4 units. The interaction of Cu cations with PO_4 units in SAPO should result in the excellent catalytic performance for the formation of HCHO, CO and H_2 in methane oxidation with O_2.

3.2 Catalytic performances of Cu/SAPO

The catalytic performance of Cu/SAPO for methane oxidation with O_2 was examined in detail. Fig. 3 shows the results for methane oxidation with O_2 over Cu/SAPO catalysts with different Cu loadings. Cu loadings in the catalysts were adjusted to be 0.3, 0.5, 1.0 or 1.5 wt%. The XRD patterns of these catalysts showed only diffraction lines due to SAPO34 as shown Fig. S7,† suggesting that Cu species were highly dispersed for all the catalysts irrespective of Cu loading.

The catalytic activity of Cu/SAPO for methane oxidation became higher with Cu loading. The amount of Cu cations in the catalyst bed was larger with the Cu loading in the catalysts since the same amount of the catalysts (0.050 g) was packed in the catalyst beds for all the reactions in Fig. 3. The selectivity to each product slightly depends on the Cu loading in the catalysts as shown in Fig. S8.† HCHO, CO and H_2 in addition to CO_2 and H_2O were formed in the reaction over all the Cu/SAPO catalysts regardless of Cu loading. Selectivities to HCHO and H_2 were decreased and instead those to CO_2 and H_2O were increased with Cu loading in the catalysts. On the other hand, the yields of HCHO, CO and H_2 for the reactions over Cu/SAPO with Cu loadings of 0.5, 1.0 and 1.5 wt% were similar. It is likely that the number of active sites for the formation of these products was not significantly increased with Cu loading. It is easily expected that Cu dimers and Cu trimers are formed in the catalysts with Cu loading. Cu monomers stabilized in SAPO catalyze methane oxidation into HCHO, CO and H_2, whereas Cu dimers and trimers preferentially form CO_2 and H_2O.

The stability of Cu/SAPO catalysts for methane oxidation at 923 K was evaluated. Fig. 4 shows the change of methane conversion and the yields of HCHO, CO and H_2 as a function of time-on-stream in methane oxidation over Cu(0.5 wt%)/SAPO at 923 K. A slight increase in the selectivities to CO, HCHO and H_2 was confirmed during the reaction over Cu/SAPO catalysts (Fig. S9†), while the methane conversion decreased slightly and gradually with time-on-stream. Thus, the yields of these products became slightly higher with time on stream of methane. These results indicate that Cu/SAPO catalysts are stable for the formation of H_2, CO and HCHO in methane oxidation with O_2 at 923 K in spite of high reaction temperatures.

The contact time of the reactants for methane oxidation over Cu/SAPO catalysts was changed in order to evaluate the contribution of successive oxidation of the primary products to product selectivity. The change of selectivity to each product was plotted as a function of W/F (W, weight of the catalyst (g); F, flow rate of the reactants (mL min^{-1})) in methane oxidation over the Cu(0.5 wt%)/SAPO catalyst at 923 K in Fig. 5. The selectivity based on C atoms to HCHO and CO decreased and that to CO_2 instead increased with an increase in W/F values. Similar to the selectivity based on C atoms, the selectivity based on H atoms to HCHO and H_2 also decreased and that to H_2O increased as W/F values increased. These results strongly suggested that HCHO, CO and H_2 are the primary products in methane oxidation with O_2 over Cu/SAPO catalysts. Note that the selectivity to CO_2 became low and it seemed to approach zero, as W/F values decreased. In contrast, the selectivity to H_2O did not approach zero at low W/F values. CH_4 would react with O_2 to form H_2O and some intermediates such as HCHO, which are adsorbed on active sites. The intermediates adsorbed on the active sites are desorbed and/or decomposed to form HCHO, H_2 and CO.

The dependence of the reaction rates of methane oxidation with O_2 over the Cu(0.5 wt%)/SAPO catalyst on the partial pressures of CH_4 or O_2 was evaluated. Fig. 6 shows the reaction rates of CH_4 against partial pressures of CH_4 or O_2. The reaction rate of CH_4 increased with increasing partial pressures of CH_4 and O_2, but its increase appears to have saturated in the high partial pressure range, indicating that methane oxidation over Cu/SAPO proceeds through the Langmuir–Hinshelwood mechanism, *i.e.*, both CH_4 and O_2 adsorb to form intermediates on the active sites on the Cu/

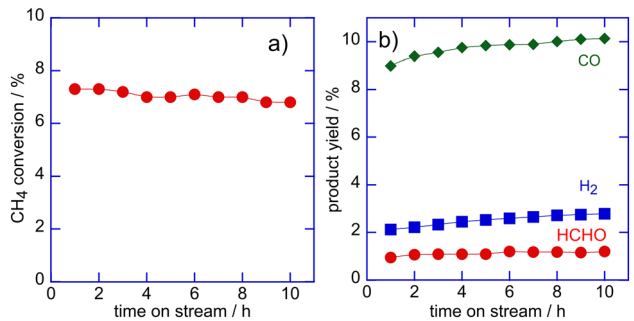

Fig. 4 Kinetic curves for CH_4 conversion (a) and yields of each product (b) in methane oxidation over the Cu(0.5 wt%)/SAPO catalyst at 923 K.

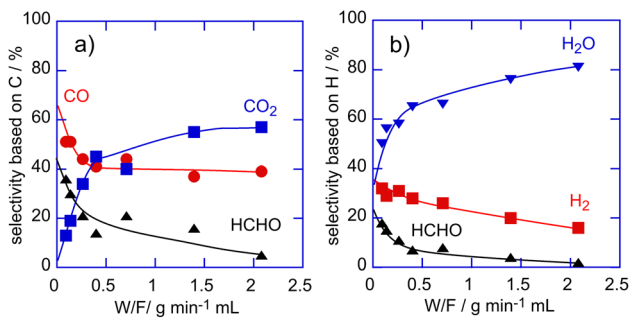

Fig. 5 Change of selectivity to each product as a function of W/F in methane oxidation over the Cu/SAPO catalyst at 923 K. a) selectivity to each product based on C, b) selectivity to each product based on H.

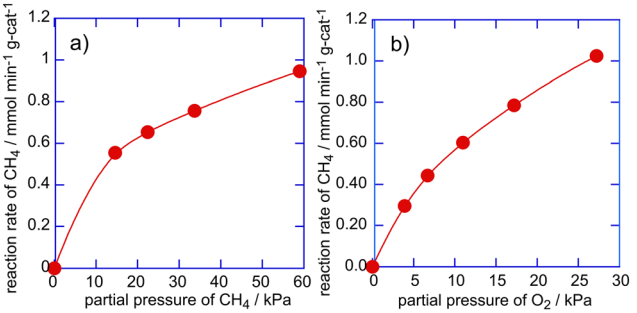

Fig. 6 Dependence of the reaction rate of methane on the partial pressure of CH_4 (a) and O_2 (b) in methane oxidation over the Cu/SAPO catalyst at 823 K.

SAPO catalyst. The reaction order of CH_4 and O_2 for the reaction rates of CH_4 was evaluated to be 0.4 and 0.6, respectively. Thus, the activation of CH_4 and O_2 on the active sites would be related to the rate determining step for methane oxidation with O_2 over the Cu/SAPO catalyst.

Finally, the structures of Cu species stabilized in SAPO, *BEA and CHA were evaluated using *in situ* UV-vis spectra.[45] The crystal structure of SAPO was the same as that of MOR. After these Cu catalysts were treated in O_2 diluted with N_2 ($O_2:N_2$ = 2:5 as the volume ratio, total flow rate = 70 mL min^{-1}) at 973 K for 1 h, diffuse reflectance UV-vis spectra for these catalysts were measured at 773 K under diluted O_2 stream. After the measurement of the spectra, mixed gases composed of CH_4 and O_2 diluted with N_2 ($CH_4:O_2:N_2$ = 2:1:4 as the volume ratio, total flow rate = 70 mL min^{-1}) were brought into contact with these catalysts at 773 K and then the UV spectra for the catalysts were measured at 773 K under the mixed gases. Fig. 7 shows the UV-vis spectra for Cu(0.5 wt%)/SAPO, Cu(0.5 wt%)/CHA and Cu(0.5 wt%)/*BEA catalysts. A strong peak at around 300 nm and a broad absorption in the range of 600 to 850 nm were observed in the UV-vis spectra for all the fresh Cu catalysts. These peaks at around 300 nm are assigned to the charge transfer from ligands to metals (LMCT) for Cu^{2+}, while the absorption in the range of 650 to 850 nm is due to the d–d transition of Cu^{2+}.[46,47] Thus, highly dispersed Cu^{2+} cations in these

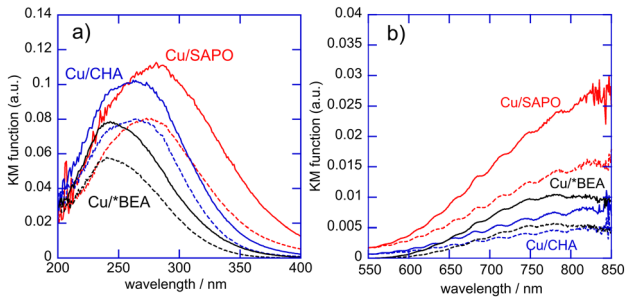

Fig. 7 *In situ* diffuse reflectance UV-vis spectra for Cu/SAPO, Cu/CHA and Cu/*BEA catalysts (a) with wavelengths from 200 to 400 nm, and (b) from 550 to 850 nm. Solid lines for the catalysts before the reactions, and dotted lines for the catalysts during methane oxidation.

catalysts are stabilized in the framework of each zeolite. It should be noted that the position of the peak due to LMCT for Cu/SAPO is different from that for Cu/CHA and Cu/*BEA, indicating that the coordination of Cu^{2+} in the zeolite frameworks is different among these Cu catalysts. The peak position of LMCT for Cu^{2+} is reported to be sensitive to their coordination, *i.e.*, the type and/or the number of anions (SiO_4, AlO_4 or PO_4) around the cations.[47] Cu^{2+} cations in Cu/SAPO are surrounded with phosphate PO_4 units in addition to AlO_4 and SiO_4 units, whereas Cu^{2+} cations in Cu/CHA and Cu/*BEA interact with SiO_4 and AlO_4 units. The intensity for the absorption due to LMCT of Cu^{2+} and the d–d transition of Cu^{2+} slightly decreased by changing the gas from O_2 to mixed gases of CH_4 and O_2. This spectral change is assignable to the reduction of a part of Cu^{2+} in the catalysts into Cu^+ during methane oxidation at 773 K.[30] The redox between Cu^{2+} and Cu^+ is related to the oxidation of methane with O_2. Cu^{2+} cations in the zeolites are reduced to Cu^+ with CH_4 molecules, and the Cu^+ cations are oxidized with O_2 to Cu^{2+} to form products such as CO and HCHO. Cu^{2+} cations dispersed in the zeolites should work as active sites for the formation of HCHO, H_2 and CO in methane oxidation with O_2. It is likely that the Cu catalysts supported on zeolites form HCHO intermediates adsorbed on the active sites. The behavior for the desorption and/or decomposition of the intermediates depends on the type of zeolite, due to differences in the number and/or strength of acid property.

Conclusions

The catalytic performance of Cu/SAPO for methane oxidation with O_2 was evaluated in the temperature range of 773–923 K. Cu/SAPO formed H_2 in addition to HCHO and CO during the reaction, and the yields of these products in the reaction over Cu/SAPO were significantly higher than those over other 3d transition metal catalysts (V, Cr, Mn, Fe, Co, Ni) supported on SAPO. In addition, Cu catalysts supported on zeolites different from SAPO (*BEA, MOR, FAU, CHA) also formed H_2, CO and HCHO during methane oxidation and the H_2 yield in the reaction over Cu/SAPO was the highest among the 3d metal/SAPO catalysts tested in this study. The interaction of Cu^{2+} and PO_4 in SAPO provides excellent catalytic performance for the partial oxidation of methane with O_2 to H_2, CO and HCHO.

Data availability

We confirm that the data supporting the findings of this study are available within the article and/or its ESI.†

Author contributions

Mana Shimakawa: conceptualization, data curation and investigation. Reiko Nagase: investigation and data curation. Ryoya Kugo: investigation and data curation. Junya Ohyama: investigation and writing – review & editing. Sakae Takenaka: conceptualization, project administration, funding

acquisition, formal analysis, investigation and writing – original draft.

Conflicts of interest

There are no conflicts to declare.

Acknowledgements

This work was supported by JSPS KAKENHI Grant Number 23K26459.

References

1 A. Demirbas, *Energy Convers. Manage.*, 2010, **51**, 1547–1561.
2 M. C. Alvarez-Galvan, N. Mota, M. Ojeda, S. Rojas, R. M. Navarro and J. L. G. Fierro, *Catal. Today*, 2011, **171**, 15–23.
3 T. V. Choudhary and V. R. Choudhary, *Angew. Chem., Int. Ed.*, 2008, **47**, 1828–1847.
4 I. V. Zagaynov, *Energy Fuels*, 2021, **35**, 9124–9136.
5 A. S. Ai-Fatesh, N. Patel, A. H. Fakeeha, M. F. Alotibi, S. B. Alreshaidan and R. Kumar, *Catal. Rev.:Sci. Eng.*, 2024, **66**, 2209–2307.
6 H. Schulz, *Appl. Catal., A*, 1999, **186**, 3–12.
7 P. Tian, P. Y. Wei, M. Ye and Z. Liu, *ACS Catal.*, 2015, **5**, 1922–1938.
8 J. Bao, G. Yang, Y. Yoneyama and N. Tsubaki, *ACS Catal.*, 2019, **9**(4), 3026–3053.
9 A. I. Olivos-Suarez, A. Szecsenyi, E. J. M. Hensen, J. Ruiz-Martinez, E. A. Pidko and J. Gascon, *ACS Catal.*, 2016, **6**, 2965–2981.
10 P. Schwach, X. Pan and X. Bao, *Chem. Rev.*, 2017, **117**, 8497–8520.
11 P. Kumar, T. A. Al-Attas, J. Hu and M. G. Kibria, *ACS Nano*, 2022, **16**, 8557–8618.
12 Y. Tang, Y. Li and F. Tao, *Chem. Soc. Rev.*, 2022, **51**, 376–423.
13 N. F. Dummer, D. J. Willock, Q. He, M. J. Howard, R. J. Lewis, G. Qi, S. H. Taylor, J. Xu, D. Bethell, C. J. Kiely and G. J. Hutchings, *Chem. Rev.*, 2023, **123**, 6359–6411.
14 M. N. Newton, A. J. Knorpp, V. L. Sushkevich, D. Palagin and J. A. van Bokhoven, *Chem. Soc. Rev.*, 2020, **49**, 1449–1486.
15 L. Tao, I. Lee and M. S. Sanchez, *Catal. Sci. Technol.*, 2020, **10**, 7124–7141.
16 M. Ravi, M. Ranocchiari and J. A. van Bokhoven, *Angew. Chem., Int. Ed.*, 2017, **56**, 16464–16483.
17 H. M. Rhoda, A. J. Heyer, B. E. R. Snyder, D. Plessers, M. L. Bols, R. A. Schoonheydt, B. F. Sels and E. I. Solomon, *Chem. Rev.*, 2022, **122**, 12207–12243.
18 J. Ohyama, A. Hirayama, Y. Tsuchimura, N. Kondou, H. Yoshida, M. Machida, S. Nishimura, K. Kato, I. Miyazato and K. Teranishi, *Catal. Sci. Technol.*, 2021, **11**, 3437–3446.
19 K. T. Dinh, M. M. Sullivan, K. Narsimhan, P. Serna, R. J. Meyer, M. Dincă and Y. Román-Leshkov, *J. Am. Chem. Soc.*, 2019, **141**, 11641–11650.
20 A. Al-Anazi, O. Bellahwel, K. C., S. Santhosh, A. E. Abasaeed, J. Abu-Dahrieh, A. H. Fakeeha, A. A. Ibrahim and A. S. Al-Fatesh, *Catalysts*, 2024, **14**, 316.
21 M. J. G. Fait, A. Ricci, M. Holena, J. Rabeah, M.-M. Pohl, D. Linke and E. V. Kondratenko, *Catal. Sci. Technol.*, 2019, **9**, 5111–5121.
22 F. Arena, N. Giordano and A. Parmaliana, *J. Catal.*, 1997, **167**, 66–76.
23 R. G. Herman, Q. Sun, C. Shi, K. Klier, C. Wang, H. Hu, I. E. Wachs and M. M. Bhasin, *Catal. Today*, 1997, **37**, 1–14.
24 A. Matsuda, T. Aihara, S. Kiyohara, Y. Kumagai, M. Hara and K. Kamata, *ACS Appl. Nano Mater.*, 2024, **7**, 10155–10167.
25 Y. Wang and K. Otsuka, *J. Catal.*, 1995, **155**, 256–267.
26 A. Matsuda, H. Tateno, K. Kamata and M. Hara, *Catal. Sci. Technol.*, 2021, **11**, 6987–6998.
27 T. Akiyama, M. Shimakawa and S. Takenaka, *Chem. Lett.*, 2022, **51**, 511–514.
28 M. Shimakawa and S. Takenaka, *Catal. Sci. Technol.*, 2023, **13**, 3859–3866.
29 T. Nash, *Biochem. J.*, 1953, **55**, 416–421.
30 J. Ohyama, Y. Tsuchimura, A. Hirayama, H. Iwai, H. Yoshida, M. Machida, S. Nishimura, K. Kato and K. Takahashi, *ACS Catal.*, 2022, **12**, 2454–2462.
31 G. Yang, X. Du, J. Ran, X. Wang, Y. Chen and L. Zhang, *J. Phys. Chem. C*, 2018, **122**, 21468–21477.
32 E. L. Uzunova, F. Göltl, G. Kresse and J. Hafner, *J. Phys. Chem. C*, 2009, **113**, 5274–5291.
33 L. Shi, J. Zhang, G. Shen, D. Fan, Y. Wen, Y. Zhao, R. Chen, M. Shen and B. Shan, *Catal. Sci. Technol.*, 2019, **9**, 1309–1316.
34 M. Prettre, C. Eichner and M. Perrin, *Trans. Faraday Soc.*, 1946, **42**, 335–339.
35 A. P. E. York, T. Xiao and M. L. H. Green, *Top. Catal.*, 2003, **22**, 345–358.
36 K. Murata, K. Arai, N. Kondo, R. Manabe, T. Yumura and S. Hosokawa, *Catal. Sci. Technol.*, 2024, **14**, 3253–3264.
37 L. Li, N. H. M. Dostagir, A. Shrotri, A. Fukuoka and H. Kobayashi, *ACS Catal.*, 2021, **11**, 3782–3789.
38 H. Kobayashi, A. Shrotri, K. Kato, A. Fukuoka and H. Kobayashi, *Catal. Sci. Technol.*, 2023, **13**, 5190–5196.
39 L. Fu, X. Li, Mi. Liu and H. Yang, *J. Mater. Chem. A*, 2013, **1**, 14592–14605.
40 Y. Li, D. An, Q. Zhang and Y. Wang, *J. Phys. Chem. C*, 2008, **112**, 13700–13708.
41 D. K. Pappas, M. Martini, M. Dyballa, K. Kvande, S. Teketel, K. A. Lomachenko, R. Baran, P. Clatzel, B. Arstad, G. Berlier, C. Labberti, S. Bordiga, U. Olsbye, S. Svelle, P. Beato and E. Borfecchia, *J. Am. Chem. Soc.*, 2018, **140**, 15270–15278.
42 H. M. Rhoda, D. P. Plessers, A. J. Heyer, M. L. Bols, R. A. Schoonheydt, B. F. Sels and E. I. Solomon, *J. Am. Chem. Soc.*, 2021, **143**, 7531–7540.
43 A. Brenig, J. W. A. Fischer, D. Klose, G. Jeschke, J. A. van Bokhoven and V. L. Sushkevich, *Angew. Chem.*, 2024, **63**, e202411662.
44 M. H. Groothaert, P. J. Smeets, B. F. Sels, P. A. Jacobs and R. A. Schoonheydt, *J. Am. Chem. Soc.*, 2005, **127**, 1394–1395.
45 Y. Tsuchimura, H. Yoshida, M. Machida, S. Nishimura, K. Takahashi and J. Ohyama, *Energy Fuels*, 2023, **37**, 9411–9418.

46 H. Li, C. Paolucci, I. Khurana, L. N. Wilcox, F. Göltl, J. D. Albarracin-Caballero, A. J. Shih, F. H. Ribeiro, R. Gounder and W. F. Schneider, *Chem. Sci.*, 2019, **10**, 2373–2384.

47 F. Göltl, S. Bhandari, E. A. Lebrón-Rodríguez, J. I. Gold, S. I. Zones, I. Hermans, J. A. Dumesic and M. Mavrikakis, *Catal. Sci. Technol.*, 2022, **12**, 2744–2748.